Hyaluronated nanoparticles deliver raloxifene to CD44-expressed colon cancer cells and regulate lncRNAs/miRNAs epigenetic cascade

Ahmed A. Abd-Rabou[1,2]* , Ahmed M. Abdelaziz[3,4], Olfat G. Shaker[5] and Ghada Ayeldeen[5]

*Correspondence:
ahmedchemia87@yahoo.com

[1] Hormones Department, Medical Research and Clinical Studies Institute, National Research Center, Dokki, Giza 12622, Egypt
[2] Stem Cell Lab, Centre of Excellence for Advanced Science, National Research Center, Dokki, Giza 12622, Egypt
[3] Ahmed Mahr Teaching Hospital (AMTH), Cairo, Egypt
[4] Supplementary General Sciences, Future University in Egypt, Cairo, Egypt
[5] Medical Biochemistry and Molecular Biology Department, Faculty of Medicine, Cairo University, Cairo, Egypt

Abstract

Background: Colorectal malignant cells (CRC) are one of the world's main causes of cancer mortality and morbidity. Notwithstanding the plenty of anti-CRC therapeutics, its prognosis remains not selective owing to cancer resistance to these therapeutics. Raloxifene (RX), a medication firstly used to treat osteoporosis, was recently licenced for the prevention of CRC. Unfortunately, due to medication resistance, many RX-based therapies are likely to become ineffective. Recently, we identified a novel method of administration to lengthen the half-life of RX by mixing it with chitosan (CS) and hyaluronic acid (HA). Thus, the rationale of the current study was to investigate how colon cancer cells were affected by RX-HA-CS nanoparticles (RX NPs) in terms of targetability, cytotoxicity, and epigenetic cascade alteration.

Results: RX NP had an entrapment efficiency (EE%) of 90.0 ± 8.12%. Compared to HCT 116 cells, Caco-2 cells were more susceptible to the cytotoxic effects of RX and its NP as well as they had a higher binding affinity to CD44 receptors compared to normal WI-38 cells. In comparison to the free RX, the RX NP's cytotoxic fold changes in HCT 116 and Caco-2 cells were 2.16 and 2.52, respectively. Furthermore, the epigenetic cascade of some noncoding RNAs was examined. Moreover, particular protein concentrations were investigated in all tested cells after application of the proposed therapies. Our results showed that the RX NP recorded higher remarkable cytotoxic impact on CRC cells compared to the free RX. Intriguingly, it was hypothesized that RX nanoparticles attacked colon cancerous cells by up-regulating miR-944 and E-cadherin (ECN) expressions, while down-regulating the expressions of PPARγ, YKL-40, VEGF, H-19, LINC00641, HULC, HOTTIP, miR-92a, miR-200, and miR-21.

Conclusions: We may conclude that the RX NP effectively targets CRC cells in vitro via altering lncRNAs and miRNAs epigenetic cascade as well as cellular uptake through CD44-expressed CRC cells.

Keywords: Raloxifene, Hyaluronic acid, lncRNA, miRNA, Colon cancer cells

Background

Colorectal cancer is a common malignancy among men (CRC). Raloxifene (RX), an oestrogen receptor-β (ER-β)-selective drug, has not been thoroughly explored in colorectal cancer. The expression of ER-β was tested in both colon HCT 116 and Caco-2 cancer cells, and it was discovered that Caco-2 cell lines have higher ER-β expression than HCT 116 cells. Scientists discovered that ER-β promotes colon cancer and that RX acts as an antagonist to ER-β, providing protection against colorectal cancer (Tolba et al. 2015).

Many RX-based therapies are likely to become unsuccessful as a result of medication resistance. We recently published a study that combined hyaluronic acid and chitosan (RX-HA-CS NPs) to upsurge the half-life of RX drug. This nano-approach was used to induce apoptosis in lung and liver cancer cell types (Almutairi et al. 2019). In the current study, we performed some modifications on the RX-HA-CS NPs and applied it against human colorectal cells to induce cytotoxicity through modulations of noncoding RNAs.

Nanoparticles (NPs) have a number of advantages over free chemotherapeutic agents, such as protection against enzymatic attacks (Suchaoin et al. 2017), resistance and cytotoxicity (Abd-Rabou et al. 2022a; Abd-Rabou and Edris. 2021, 2022; Hashim et al. 2022), transportation, penetration, tumour site retention, and low pharmacokinetics (Bikiaris et al. 2009). NPs can improve the therapeutic efficacy of standard anticancer medications while reducing negative effects (Zhang et al. 2017). Encapsulation of free anticancer medicines in polymeric NPs is an excellent way to do that. Chitosan NPs allow hydrophobic medications to be loaded in the core of the NPs, allowing for long-term release from the particle's shell (El-Hamed et al. 2022). Surprisingly, these NPs improve the loaded medicines' solubility and biocompatibility (Zhang et al. 2017).

Hyaluronic acid (HA) was discovered to target the cluster of differentiation-44 (CD44) receptor for cancer therapy. All mammalian cells have the glycoprotein CD44 on their surface, which is involved in a number of biological activities. Although CD44 is overexpressed in many cancers, such as lung (Almutairi et al. 2019), investigations have concentrated on ways to target it in an effort to enhance drug delivery, distinguish between undiseased and cancerous cells, and lessen toxicity on the undiseased cells (Mattheolabakis et al. 2015).

Since RX is water insoluble and has a poor bioavailability, the FDA approved it as antibreast cancer candidate (Abd-Rabou et al. 2017; Bikiaris et al. 2009).

As a result, RX must be placed onto an appropriate nanocarrier to improve its biocompatibility and release profile. RX-loaded polymeric nanoparticles that allowed for a rapid initial release rate followed by very gradual drug release rates were created (Fontana et al. 2014; Sporn et al. 2004).

Epigenetic cascade of lncRNAs (nominated; long noncoding RNAs) and miRNAs (nominated; micro-RNAs) are two types of noncoding RNAs (Meng et al. 2017). lncRNAs are used as epigenetic biomarkers in the early stages of CRC diagnosis. Most lncRNAs are associated to CRC progression/oncogenes or tumour suppressor genes (Siddiqui et al. 2019). They also influence cancer by multimechanistic approaches involving miRNA modulation, cell proliferation, death, and invasion control (Lizarbe et al. 2017).

LncRNAs H-19, HOTTIP, LINC00641, and HULC have important role in colon cancer. The EMT, an epithelial-to-mesenchymal transition, is activated by H-19 that has a

role in mammalian development (Wang et al. 2016). H-19 was overexpressed in a number of cancers. (Raveh et al. 2015). HOTTIP was also overexpressed in cancer especially in breast cancer (Abdelaleem et al. 2012). Cancer cell metastasis was regulated by HULC. Its expression was increased in a number of cancers, including liver cancer and CRC (Shaker et al. 2017).

LINC00641 was increased in CRC, indicating that it is a predictor of overall CRC survival. HCT116 and SW620 cells' proliferative and migratory activity are impaired when LINC00641 is knocked out. According to a study published in 2021 (Xue et al. 2021), LINC00641 increases CRC cell growth and invasion via miRNAs.

The miR-200 group of genes could be utilized as diagnostic marker for cancer. It was linked to cancer progression, angiogenesis, and survival of malignant cells (Carter et al. 2019). As miRNAs are associated to progressive phases of colon cancer, miR-21 and miR-92a play key roles in CRC. One of the most important indicators of CRC is miR-21 (Schee et al. 2012). MiR-944 is a critical marker in cancer because it limits the ability of cancer cells to infiltrate (Liu et al. 2016).

To increase RX medication delivery, the current study takes advantage of features, such as selective HA targeting against CD44 receptors and the utilization of chitosan as a polymeric nanocarrier. This aims at investigating the anticancer potential of RX, RX-CS NPs (two formulas F1 and F2), and RX-HA-CS NPs against human colorectal HCT 116 and Caco-2 cancerous cells versus normal WI-38 cells. The aptitude of these regimens inhibits CRC proliferation via epigenetic cascade alteration and connection with CD44 receptors on the cancer cells.

Materials and methods

Materials

Polyvinyl alcohol (PVA), 3-(4,5-dimethylthiazol-2-yl)-2,5-diphenyltetrazolium bromide (MTT), N-hydroxysuccinimide (NHS), raloxifene hydrochloride (RX), hyaluronic acid (HA), chitosan (CS, Mw: 50 KDa, deacetylated chitin), and 1-ethyl-3-(3-dimethylaminopropyl)carbodiimide (EDC) were obtained from (Sigma-Aldrich, USA). Dulbecco's modified Eagle's medium (DMEM) and medium supplements were got from (Life Technologies, USA). The miRNeasy, RT2 First-Strand, and RT2 SYBR Green were obtained from Qiagen, USA. TaqMan MicroRNA RT kit and Thermo Scientific Maxima SYBR Green qPCR Master mix (ThermoFisher, USA). The ELISA of PPAR-γ (i.e. peroxisome proliferator-activated receptor γ) was got from (WKEA, USA). The ELISA kit of YKL-40 (i.e. chitinase 3-like 1) was purchased from (R&D Systems, USA). The kit of ECN was got from (MyBiosource, USA). The VEGF kit was obtained from (AviBion, Finland).

Preparation of nanoparticles

CS nano-voids (F1 and F2)

Chitosan (CS) nanoparticles, without loading a drug called CS nano-void, were synthesized by single emulsion solvent evaporation method (Abd-Rabou and Ahmed. 2017; Parveen et al. 2011) with some alterations. Briefly, 12% *w/w* of CS 1% acetate was synthesized. The CS was added to 12 ml of 2% *w/v* PVA. Formulas 1 and 2 (F1 and F2) of the CS nano-voids were prepared by different ratios of the CS and PVA solutions (F1; 1: 0.1 and F2; 1: 0.3, respectively).

RX-CS NPs (F1 and F2)

5 mg/mL Raloxifene (RX) was dissolved in DMSO to prepare RX solution. RX solution was added to CS and PVA solution prior emulsification to prepare F1 and F2 of the RX-CS NPs, using energy of pulses $=55W$ from a probe sonicator (Vibracell Sonics, USA) for 2 min. The organic solvent was allowed to evaporate overnight while the emulsion was agitated.

F1 selection

We selected formulation F1 from the two CS nano-voids to synthesize HA-CS nano-void and encapsulate RX. F1 was selected because it represents lower nano-size and polydipersity index (98.5 ± 7.3 nm, 0.01 ± 0.00) than F2 (180.5 ± 5.5, 0.51 ± 0.00), with stable zeta potential readings (see the Results).

HA-CS nano-void and labelled NPs

Functionalization of HA on the surface of CS nano-voids to prepare HA-CS nano-void was performed. 3.75 mM NHS and 1.5 mM EDC were stirred for 1 h to initiate covalent bonding between the CS NPs and HA solution in the ratios of 1: 0.5. This new suspension was stirred overnight at 4 °C, after that new CS HA-functionalized CS NPs (HA-CS nano-void) were approached.

Labelled NPs (i.e. HA-exposed NPs labelled with CD44 antibody attached to Alexa Flour 488) were prepared with the same EDC/NHS stimulation procedure mentioned above with the addition of 0.05% (w/w) anti-CD44 antibody tagged with the fluorescent dye; the resultant NPs were then exposed to a dialysis procedure to remove the unconjugated dye.

RX-HA-CS NPs (RX NP)

Preparation of the RX-HA-CS NPs was approached through two subsequent steps. Step 1: 5 mg/mL RX to prepare RX solution. This solution was added to CS and PVA solutions prior emulsification to prepare the RX-CS NPs (F1), using probe sonication. Step 2: Functionalization of HA on the surface of the RX-CS NPs (F1) to prepare RX-HA-CS NPs (RX NP) was performed. 3.75 mM NHS and 1.5 mM EDC were stirred for 1 h to initiate covalent bonding between the nanocapsule and HA solution in the ratios of 1:0.5. This new RX-HA-CS NPs was stirred overnight at 4 °C.

NPs purification and sterilization

Excess amounts of PVA, acetic acid, and organic solvents were removed from the mixture by ultracentrifugation at $50 \times 10^3 \times g$ (4 °C) using (Sorvall Ultraspeed Centrifuge, USA) for 20 min, followed by washing. We also utilized 0.2–0.45 µm membrane filters. This method was used for sterilization through removing microorganisms exist in liquid nanoparticles.

Encapsulation efficiency (EE%) measurement

Dialysis assay was utilized for eradicating the impurities and the nonconjugated RX with RX-CS NPs (F1), RX-CS NPs (F2), and RX-HA-CS NPs using a specific

membrane from Spectrum Laboratories, USA (with MWCO equal to 25KDa). The concentrations of free RX were measured using this method. Using UV-based BMG Labtech, the free and conjugated forms of RX were found using a variable wavelength detector. Throughout the range of standard concentrations, the calibration curves for measurement of these chemicals were linear. After the dialysis assay, EE% was ultimately calculated.

Size and zeta potential

The nanoparticle size as well as zeta potential analyses of RX, RX-CS NPs (F1), RX-CS NPs (F2), and RX-HA-CS NPs were achieved by Malvern ZetaSizer. 1 mL of the samples was filled in the sizing clear cuvette for measuring the size distribution and zeta potential, which were analysed at 25 °C with a Malvern apparatus (Westborough, Massachusetts).

In vitro RX release experiment

The in vitro RX released from the prepared RX-CS NPs (F1), RX-CS NPs (F2), and RX-HA-CS NPs was measured using dialysis technique. The NP of RX, corresponding to 250 mg, was administered in a dialysis sac, and it was induced by submerging the membrane into a graduated beaker containing 500 mL of PBS with pH 6.8. NPs were swirled continuously at 50 rpm and 37 °C. 5 mL of receptor media was sampled at set intervals throughout a course of more than 24 h to quantify the amount of drug released. 5 mL of PBS with pH 6.8 was provided to the beaker. A UV operating device was used at 233 nm to measure the amount of RX emitted in the buffer solution (Chinnaiyan et al. 2018).

Cell culturing

Human CRC cell lines (HCT116 and Caco-2) in addition to normal cells (WI-38) were obtained from VASCERA Institute in Egypt which purchased them from the American Type Culture Collection Center. In cell culture, DMEM with glucose was used. 1% L-glutamine and 10% FBS supplements were added to the complete media. CO_2 incubator was used to maintain the cells.

Cytotoxicity

RX, RX-CS NPs (F1), RX-CS NPs (F2), and RX-HA-CS NPs were assayed by MTT dye **(**Van Meerloo et al. 2011**)** using Caco-2, HCT116, and WI-38 cells. On 96-well plates, these cells were applied at a density of 1×10^4 cells per well. All RX regimens were administered to the medium over these cells at the aforementioned doses (0, 40, 60, 80, and 100 µM), and the cells were then incubated for 24 and 48 h. As a comparison for RX-loaded NPs, culture media treated with nano-void (i.e. nanocapsule without entrapped RX) was used as a control. Free RX-treated cells, on the other hand, were normalized to untreated control cells (zero concentration represented in the cytotoxicity graphs).

After 24 h and 48 h incubation, 5 mg MTT dissolved in 1 mL PBS was applied to each well and the cells were incubated for 4 h then washed. Absorbance was detected at 540 nm after adding 100 mL of DMSO to the cells and the readings were taken by BMG reader (Germany). Cell proliferation (%) was measured and compared to the controls.

IC$_{50}$, cytotoxic, and IC$_{50}$ fold changes measurement

Using OriginPro tool (USA), a polynomial fitting experiment was used to determine the IC$_{50}$ values of the malignant cells Caco-2 and HCT116 in response to various therapies. The cytotoxic and IC$_{50}$ of all RX-based nano-regimens versus the free RX over the proposed cell lines were calculated over 24 h and 48 h treatment incubation times.

The cytotoxic fold change represents the IC$_{50}$ of the free RX divided by the IC$_{50}$ of each nano-platform to calculate the cytotoxic fold change between the RX-encapsulated nanoparticles versus the free counterpart (RX). The IC$_{50}$ fold change represents the IC$_{50}$ of each nano-platform divided by free RX to calculate the fold times in IC$_{50}$ values between the RX-encapsulated nanoparticles compared to the free counterpart (RX).

Specific binding affinity of the labelled NPs with the CD44 receptor

The binding affinities of the labelled HA NPs with CD44 Antibody-attached with Alexa Flour 488 on Caco-2, HCT116, and WI-38 cell lines were investigated after 4 and 24 h via flow cytometry apparatus. To accomplish that task, we followed the process mentioned in details in our previously published paper (Abd-Rabou et al. 2022b). 2×10^5 Caco-2, HCT116, and WI-38 cells were incubated in 5 mL binding buffer and 1 mg/mL BSA dissolved in PBS, followed by washing with PBS. 500 µL binding buffer was added to the proposed cells achieving flow cytometry (BD Cytometry System). The elevated mean intensity of the proposed cells bound with the Alexa Flour 488 was tracked.

Epigenetic experiments

Total RNA extraction

The miRNeasy extraction kit was utilized to get total RNA from colon cancer cells as well as the normal one. One million of these cells were seeded primarily with suitable conditions. Cells with RX and RX-HA-CS NPs (RX NP) were seeded. We used the IC$_{50}$ dosages for the epigenetic application. After 24 h incubation, extracted RNAs were used for testing the expression levels of both lncRNAs, including H-19, HOT-TIP, LINC00641, and HULC, as well as miRNAs, including miR-92a, miR-200a, miR-21, and miR-944.

Reverse transcription

The RNA of these three cell types was reverse transcribed via RT2 First-Strand Kit for testing lncRNAs, while the TaqMan MicroRNA Reverse transcription kit was used for Reverse transcription of miRNAs.

Real-time PCR for LncRNAs

qRT-PCR of the long noncoding gene (LncRNAs) expression was done using the RT2 SYBR Green PCR kit. We used Rotor Gene Q System (Qiagen) for that purpose. 20 µL reaction mixture was prepared with the following settings for all lncRNA genes: 95 °C

Table 1 Primers of lnRNAs and miRNAs

Primers	Noncoding RNAs
F: 5′-CCTAAAGCCACGCTTCTTTG-3′ R: 5′-TGCAGGCTGGAGATCCTACT-3′	HOTTIP LnRNA
F: 5′-TCAGCTCTGGGATGATGTGGT-3′ R: 5′-CTCAGGAATCGGCTCTGGAAG-3′	H-19 LnRNA
F:5′-ATC TGC AAG CCA GGA AGA GTC-3′ R: 5′-CTT GCT TGA TGC TTT GGT CTGT-3′	HULC LnRNA
F: 5′-CACTTTTGCAGACCCTCACA-3′ R: 5′-ACTTGACGGGTGGATTCTTG-3′	LINC00641 LnRNA
F: 5′-CCCTTCATTGACCTCAACTA-3 R: 5′-TGGAAGATGGTGATGGGATT-3′	GAPDH Housekeeping gene of LnRNAs
F: 5′- TAACACTGTCTGGTAACGATGT-3′ R: 5′- ATCGTTACCAGACAGTGTTATT-3′	miR-200a
F: 5′-CTCAACTGGTGTCGTGGAGTCGGCAATTCAGTTGATACAGGCCG-3′ R: 5′-ACACTCCAGCTGGGTATTGCACTTGTCCC-3′	miR-92a
F: 5′-CTAAGACCTGTGGAATGGC-3′ R: 5′-CTCAAAGATGTCATTGCC-3′	miR-21
F: 5′-CCGCCAAATTATTGTACATCGGATGAG-3′ R: 5′-CCAGTGCAGGGTCCGAGGTA-3′	miR-944
F: 5′- CTCGCTTCGGCAGCACATTTT-3′ R: 5′- AACGCTTCACGAATTTGCGT-3′	U6 Housekeeping gene of miRNAs

F: Forward primer

R: Reverse Primer

for 10 min, followed by 40 cycles at 95 °C for 15 s and 60 °C for 60 s. The expression values of the four lncRNAs after RX and RX-HA-CS NPs (RX NP) applications were normalized using GAPDH as a housekeeping/reference gene. The equation $2^{-\Delta\Delta Ct}$ was utilized to measure the FCs. The FC of the healthy group was assumed as 1. Table 1 shows the primers used for the LncRNAs.

Real-time PCR for miRNAs
The expression levels of the proposed miRNAs were quantified upon treatments with RX and RX-HA-CS NPs (RX NP) using Thermo Scientific Maxima SYBR Green qPCR Master mix according to the manufacturer's rules. The cycling conditions were as follows: 94 °C for 10 min, followed by 40 cycles at 94 °C for 15 s, 55 °C for 30 s, and 70 °C for 30 s. U6 was used as a housekeeping gene for miRNAs. Table 1 shows the primers used for the miRNAs.

Protein levels measurement
One million cells of all proposed cell lines were applied into tissue culture flasks. The IC_{50} doses from the cytotoxicity experiment were used to accomplish this experiment. Cell supernatants were collected during 24 h incubation period in order to perform an ELISA protein-level measurement.

PPAR-γ Quantitation
The ELISA kit was used to determine the concentration of PPAR- γ in the media in a quantitative manner. The solid-phase enzyme immunoassay (EIA) was used in accordance with the manufacturer's instructions. The relevant antibody is bound by PPAR- γ,

which is found in media and standards. The bound PPAR-γ is recognized immunologically by a conjugate/antigen/antibody complex. At 450 nm, the yellow colour's intensity was spectrophotometrically recorded.

YKL-40 Quantitation
The ELISA method to measure YKL-40 levels was carried out in accordance with the manufacturer's instructions. The quantitative sandwich EIA technique is used in this experiment. The amount of YKL-40 bound determines how the colour develops. At 450 nm, the colour intensity is measured after the colour development has been stopped.

ECN Quantitation
The quantitative sandwich procedure is used in the ECN ELISA kit. An ECN-specific monoclonal antibody has been precoated on the microtitre plate. The microtitre plate wells are filled with standards or samples. To measure the amount of ECN present in the sample, a standardized preparation of ECN-specific HRP-conjugated polyclonal antibody is applied to each well. This "sandwiches" the ECN immobilized on the plate. The enzyme substrate reaction is stopped by the addition of a sulfuric acid solution, and the colour shift at 450 nm is then measured spectrophotometrically.

VEGF Quantitation
VEGF levels were measured its specific ELISA kit in vitro in cell culture supernatants in a quantitative manner. At 450 nm, the colour intensity is quantified after the colour development has been stopped.

Statistical analysis
All assays were repeated in three separate experiments, and only representative data are presented. Comparisons between controls and nonencapsulated and encapsulated RX-treated groups were made using a two-tailed Student's *t*-test. # represents highly significant difference ($p < 0.01$) between untreated CRC and WI-38 cells, @ represents significant difference ($p < 0.05$) between treated and untreated CRC cells, as well as * represents high significant difference ($p < 0.01$) between treated and untreated CRC cells.

Results
NPs Characterization
The chemical structuring of the RX-CS and RX-HA-CS nanoparticles were schemed through sonication of CS, PVA, and RX forming the RX-CS, followed by functionalization of HA on the surfaces of the RX-CS NPs synthesizing the RX-HA-CS nanoparticles using NHS and EDC technique (Fig. 1A).

The TEM images of the RX-CS (F1), RX-CS (F2), and RX-HA-CS NPs are illustrated in Fig. 1B–D, respectively. TEM images of the raloxifene-loaded nanoparticles showing rounded NPs with shell either with CS (Fig. 1B, C) or CS linked with HA chains (Fig. 1D). Figure 1D, a magnified RX-HA-CS NPs, shows the encapsulated drug (RX) inside the core and a rounded shell of CS bound with chains of HA that target cancer cells through the overexpressed CD44 receptors on their membranes.
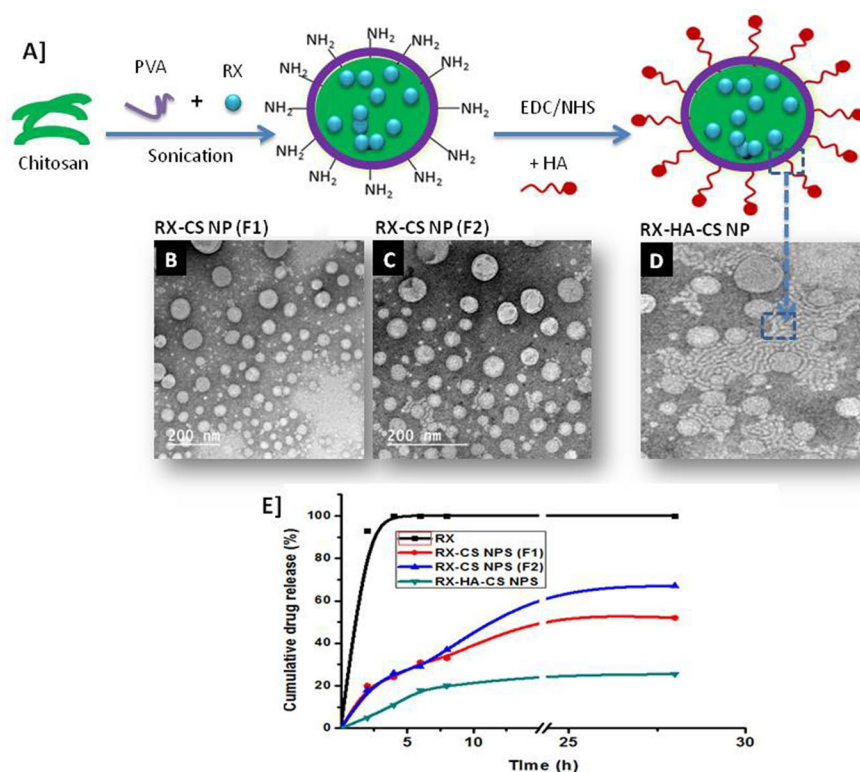
Fig. 1 Chemistry, TEM imaging, and cumulative drug release of nanoparticles. **A**] RX-CS NPs and RX-HA-CS NPs schematic diagram of their preparation, **B**, **C**, **D**] TEM images of the raloxifene synthesized nanoparticles. **B**] TEM image of formula 1 of the RX-CS NPs (F1), **C**] TEM image of formula 2 of the RX-CS NPs (F2), **D**] A magnified RX-HA-CS NPs shows the encapsulated drug (RX) inside the core and a rounded shell of CS linked with chains of HA that target cancer cells through the overexpressed CD44 receptors on their membranes. **E**] Cumulative drug release profiling of RX, RX-CS NPs (F1), RX-CS NPs (F2), and RX-HA-CS NPs. *RX* raloxifene, *HA* hyaluronic acid, *CS* chitosan, *NPs* nanoparticles

Six nano-formulations were prepared; three of them are nano-voids; without encapsulated RX [CS NPs (F1), CS NPs (F2), and HA-CS NPs], as well as three of them are nano-RX [RX-CS NPs (F1), RX-CS NPs (F2), and RX-HA-CS NPs]. For CS NPs (F1), we observed that it had the lowest average nano-size and polydipersity index (98.5 ± 7.3 nm, 0.01 ± 0.00), and good stability (highly positive-charged zeta potential $+ 14.5 \pm 3.2$ mV), which reflects highly stable particles. For CS NPs (F2), we observed that it had nano-size and polydipersity index (180.5 ± 5.5 nm, 0.51 ± 0.00) higher than F1, as well as negative-charged zeta potential $- 8.1 \pm 2.5$ mV, that reflects stable particles. Accordingly, we used the F1's preparation method to synthesize the HA-CS NPs (nano-void). It was seen that HA-CS NPs had nano-size and polydipersity index (118.2 ± 7.7 nm, 0.01 ± 0.00) higher than F1, as well as highly negative-charged zeta potential $- 14.5 \pm 5.1$ mV, that reflects stable particles (Table 2).

For RX-CS NPs (F1), it was observed that it had the lowest average nano-size and polydipersity index (102.5 ± 5.5 nm, 0.01 ± 0.00) among the RX-loaded NPs, and good stability (highly positive-charged zeta potential $+ 29.6 \pm 4.06$ mV), which reflects highly stable particles with EE% $= 89.5 \pm 4.12$% of RX inside the NPs. For RX-CS NPs (F2), we observed that it had nano-size and polydipersity index (212.5 ± 6.5 nm, 0.03 ± 0.00), as well as negative-charged zeta potential $- 9.5 \pm 1.02$ mV, that reflects stable particles

Abd-Rabou *et al. Cancer Nanotechnology*   (2023) 14:32

Page 10 of 23

Table 2 Average of size, polydipersity index (PDI), zeta potential (ZP) and entrapment effeciency (EE) of the synthesized nanoparticles

NPs type	Ratio			Mean ± SE			EE, %
	CS	PVA	HA	Size, nm	PDI	ZP, mV	
CS NPs (F1) (nano-void)	1	0.1	–	98.5 ± 7.3	0.01 ± 0.00	+ 14.5 ± 3.2	–
CS NPs (F2) (nano-void)	1	0.3	–	180.5 ± 5.5	0.51 ± 0.00	− 8.1 ± 2.5	–
HA-CS NPs (nano-void)	1	0.1	0.5	118.2 ± 7.7	0.01 ± 0.00	− 14.5 ± 5.1	–
RX-CS NPs (F1)	1	0.1	–	102.5 ± 5.5	0.01 ± 0.00	+ 29.6 ± 4.06	89.5 ± 4.12
RX-CS NPs (F2)	1	0.3	–	212.5 ± 6.5	0.03 ± 0.00	− 9.5 ± 1.02	64.1 ± 3.81
RX-HA-CS NPs	1	0.1	0.5	114.5 ± 5.6	0.04 ± 0.01	-35.3 ± 5.2	90.0 ± 8.12

Data are represented in term of mean ± standard error (SE), n = 3

PDI polydipersity index, *ZP* zeta potential, *EE%* entrapment effeciency, *RX* raloxifene, *HA* hyaluronic acid, *CS* chitosan, *NPs* nanoparticles

with EE% = 64.1 ± 3.81% of RX inside the NPs. It was observed that RX-HA-CS NPs had low nano-size and polydipersity index (114.5 ± 5.6 nm, 0.04 ± 0.01), as well as highly negative-charged zeta potential − 35.3 ± 5.2 mV, that reflects stable particles with EE% = 90.0 ± 8.12% of RX inside the NPs (Table 2).

In vitro RX release

The cumulative proportions of RX released from RX-CS NP (F1), RX-CS NP (F2), and RX-HA-CS NP versus the free RX itself over 28 h were approached (Fig. 1E). For free RX, ~ 100% of it was clearly dissolved and totally released outside the dialysis from the 1st hr of preceding the experiment and it be fixed at ~ 100% over the 28 h. For the RX-HA-CS NP, ~ 20.0% of the entrapped RX was released after 6 h of preceding the experiment with the best sustained release profiling, and it be relatively fixed at ~ 20.0% over the 28 h. The two formulas of the RX-CS NPs showed the same release profiles from 1 to 6 h, reaching around ~ 30.0% of the entrapped RX. After 6 h, the release of the RX increased until reaching the maximum (~ 65% for F2 and ~ 50% for F1) at 24 h.

Cellular binding and uptake

Cancers, including colon, have CD44 receptors overexpression on their cell surfaces. We proposed to inspect if cell-surface CD44 expression was exist in human Caco-2, HCT116, and WI-38 cells, because HA acts as a binding moiety to this receptor (Almutairi et al. 2019). Using flow cytometry apparatus, the treated cells with anti-CD44-Alexa Flour 488-labelled HA NPs were examined. It was observed that CD44 was overexpressed on the cell surfaces of human colon Caco-2 cancerous cells compared to human colon HCT116 cancerous cells, while minimally exist or approximately absent on the normal cell surfaces (WI-38 cells) (Fig. 2A–C). To choose whether colon cancer cell was responsive to the targeted therapy both cancerous cells were incubated for 4 h and 24 h incubation periods.

During the initial course of anticancer therapy with the labelled NPs, we used the incubation period of 4 h to examine the binding affinity between the HA NPs and the CD44 expression on the membrane of Caco-2, HCT116, and WI-38 cell lines. We noticed that
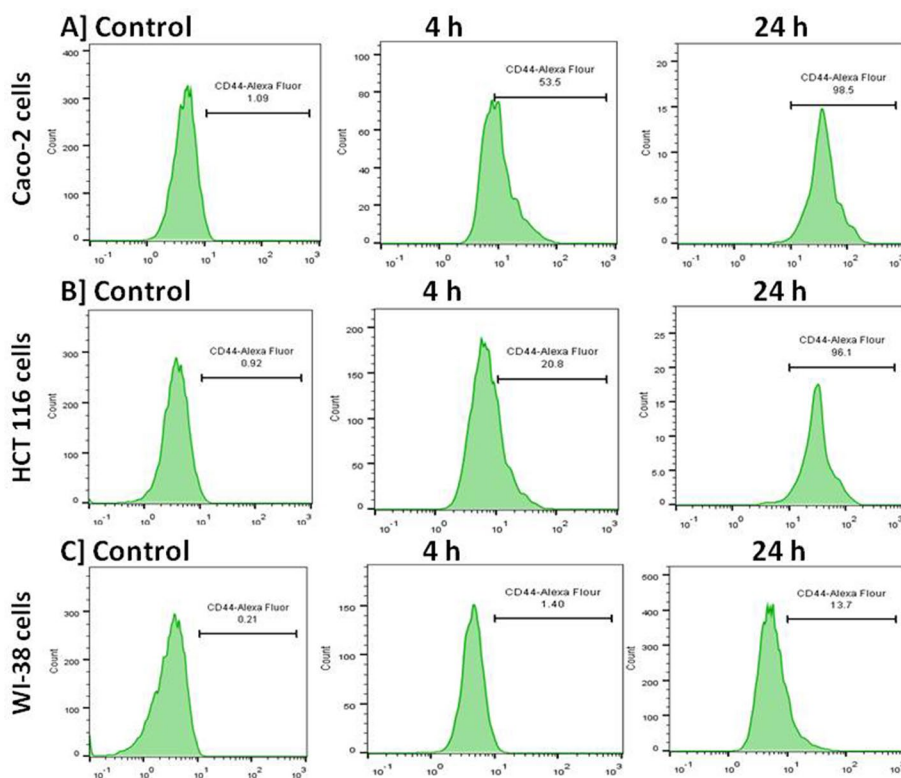
Fig. 2 CD44 expression on the proposed cells and the binding affinity of HA-CS NPs towards Caco-2 (**A**), HCT116 (**B**), and WI-38 (**C**) cell lines. Graphs showed that the NPs attached to CD44-expressed membranes of Caco-2 cells higher than HCT 116 cells, noting slight attachment with WI-38 cells

the binding affinities of Caco-2, HCT116 and WI-38 cells at the primary stage were (53.5%, 20.8%, and 1.4%, respectively) compared to the control.

After 24 h incubation with the labelled NPs, the cells get remarkably internalized inside the colorectal cancerous Caco-2 and HCT116 cells and almost bound to the expressed intracellular CD44 in both human colorectal cancer cells (98.5% and 96.1%, respectively). Intriguingly, the expression of the intracellular CD44 receptors on WI-38 cells was minimum around 13.7% (i.e. negative expression).

These observations led to nanoparticles internalization (i.e. cellular uptake) inside the cancerous cells causing cytotoxicity while sparing normal cells without internalization and damaging.

Anticancer activity

Figures 3, 4, and 5 show the anticancer effects of RX, RX-CS NPs (F1), RX-CS NPs (F2), and RX-HA-CS NPs therapeutic regimens on colorectal cancerous Caco-2 (Fig. 3), HCT 116 (Fig. 4), and WI-38 (Fig. 5) cell lines. Part "A" of each figure represents 24 h incubation period and part "B" represents 48 h incubation period of the cells with the therapeutic regimens. The zero dosage of the therapeutic regimens in all figures represent either untreated CRC cells compared to RX or treated CRC cells with nano-voids [NPs without RX; CS NPs (F1), CS NPs (F2), and HA-CS NPs] compared to RX-based nano-regimens [RX-CS NPs (F1), RX-CS NPs (F2), and RX-HA-CS NPs].
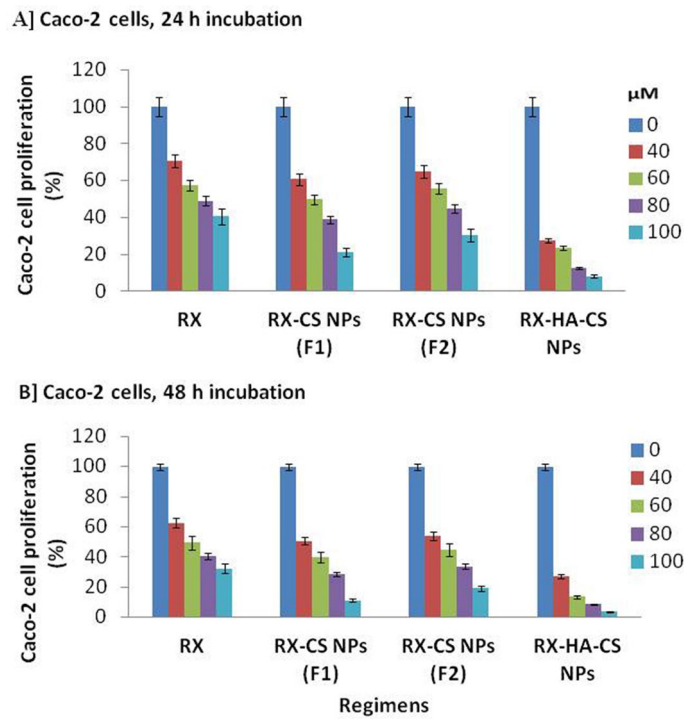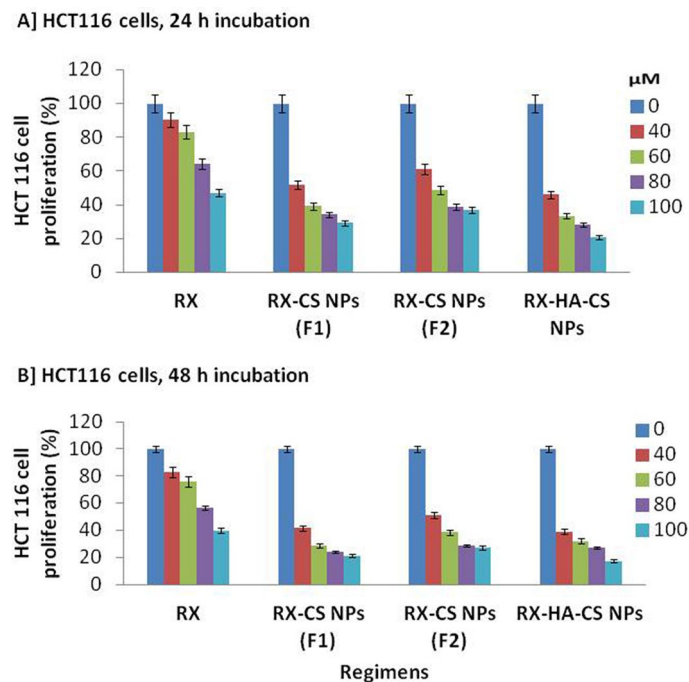
Fig. 3 Caco-2 cancer cell proliferation. The effect of RX-based free and nano-therapeutic regimens (RX, RX-CS NPs (F1), RX-CS NPs (F2), and RX-HA-CS nanoparticles on colorectal cancerous cell line (Caco-2)). The cells were treated with these free and nano-regimens using different doses ranging from 0 μM "control" to 100 μM over 24 h (**A**) and 48 h (**B**). RX: raloxifene; HA: hyaluronic acid; CS: chitosan; NPs: nanoparticles

Fig. 4 HCT116 cancer cell proliferation. The effect of RX-based free and nano-therapeutic regimens (RX, RX-CS NPs (F1), RX-CS NPs (F2), and RX-HA-CS nanoparticles on colorectal cancerous cell line (HCT116)). The cells were treated with these free and nano-regimens using different doses ranging from 0 μM "control" to 100 μM over 24 h (**A**) and 48 h (**B**). RX: raloxifene; HA: hyaluronic acid; CS: chitosan; NPs: nanoparticles
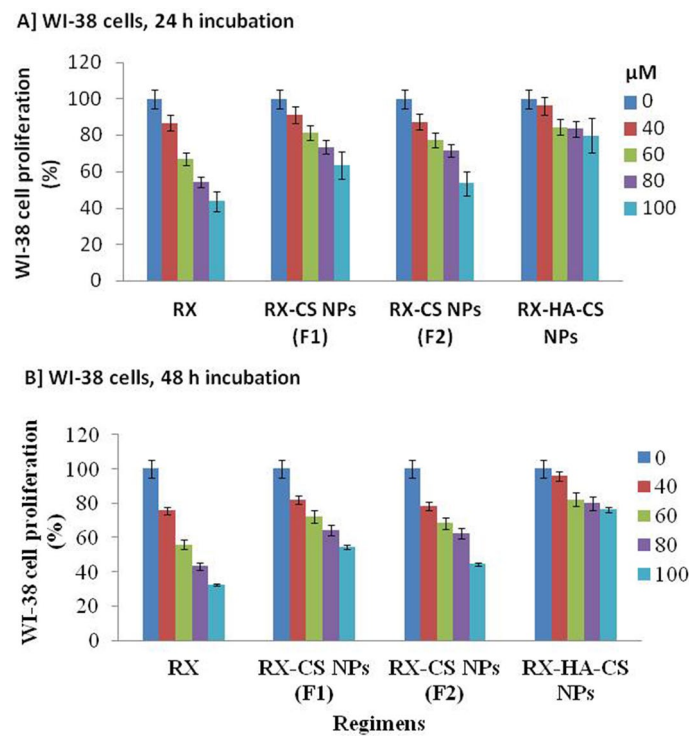
Fig. 5 WI-38 normal cell proliferation. The effect of RX-based free and nano-therapeutic regimens (RX, RX-CS NPs (F1), RX-CS NPs (F2), and RX-HA-CS nanoparticles on WI-38 cells). The cells were treated with these free and nano-regimens using different doses ranging from 0 μM "control" to 100 μM over 24 h (**A**) and 48 h (**B**). *RX* raloxifene, *HA* hyaluronic acid, *CS* chitosan, *NPs* nanoparticles

Table 3 24 h incubation half inhibitory effect (IC_{50}) of the free and nano-RX regimens and their cytotoxic and IC_{50} fold changes

Parameters	Cell lines	Free and nano-regimens			
		RX	RX-CS NPs (F1)	RX-CS NPs (F2)	RX-HA-CS NPs
IC_{50}, μM	Caco-2 cells	64.07	56.31	61.06	25.45
	HCT 116 cells	86.79	45.59	54.10	40.22
	WI-38 cells	76.30	ND	ND	ND
Cytotoxic fold	Caco-2 cells	Ref.	1.14	1.05	2.52
	HCT 116 cells	Ref.	1.90	1.60	2.16
	WI-38 cells	Ref.	0.76	0.76	0.76
IC_{50} fold	Caco-2 cells	Ref.	0.88	0.95	0.40
	HCT 116 cells	Ref.	0.53	0.62	0.46
	WI-38 cells	Ref.	ND	ND	ND

The cytotoxic fold change represents the IC_{50} of the free RX divided by the IC_{50} of each nano-platform to calculate the cytotoxic fold change between the RX-encapsulated nanoparticles versus the free counterpart (RX). The IC_{50} fold change represents the IC_{50} of each nano-platform divided by free RX to calculate the fold times in IC_{50} values between the RX-encapsulated nanoparticles compared to the free counterpart (RX)

Caco-2 and HCT 116 cells: human colorectal cell lines, *IC_{50}* the average of colorectal cancer cell's half inhibitory effect; *RX* raloxifene, *HA* hyaluronic acid, CS: chitosan, *NPs* nanoparticles

There was a statistically significant decrease ($p < 0.05$) of all free RX and nano-based regimens for Caco-2 (Fig. 3) and HCT116 (Fig. 4) cells but nonsignificant decrease ($p > 0.05$) for normal WI-38 cells (Fig. 5), especially for treated cells with the RX-HA-CS

Table 4 48 h incubation half inhibitory effect (IC_{50}) of the free and nano-RX regimens and their cytotoxic and IC_{50} fold changes

Parameters	Cell lines	Free and nano-regimens			
		RX	RX-CS NPs (F1)	RX-CS NPs (F2)	RX-HA-CS NPs
IC_{50}, μM	Caco-2 cells	55.99	46.23	49.99	20.61
	HCT 116 cells	79.38	35.27	44.03	36.65
	WI-38 cells	65.14	77.41	74.65	ND
Cytotoxic fold	Caco-2 cells	Ref.	1.211	1.120	2.717
	HCT 116 cells	Ref.	2.251	1.803	2.166
	WI-38 cells	Ref.	0.841	0.873	ND
IC_{50} fold	Caco-2 cells	Ref.	0.826	0.893	0.368
	HCT 116 cells	Ref.	0.444	0.555	0.462
	WI-38 cells	Ref.	1.188	1.146	ND

NPs. Increasing time of incubation is directly proportional with increasing cytotoxicity on cancerous cells, but the RX-HA-CS NP regimen did not kill normal cells more, may be due to the absence of the CD44 receptors on the WI-38 cells (Table 3; 24 h incubation and Table 4; 48 h incubation).

The IC_{50} values, cytotoxic, and IC_{50} fold changes of all nano-regimens versus the free RX over human Caco-2 and HCT116 cells as well as normal WI-38 cells are shown in Tables 3 and 4 for 24 h and 48 h incubation periods, respectively.

For 24 h incubation, the free anticancer drug RX detected IC_{50} values equal to 64.07 μM, 86.79 μM, 76.30 μM for Caco-2, HCT116, and WI-38 cells, respectively. Meanwhile, there were undetectable IC_{50} values (more than 100 μM) for normal WI-38 cells upon RX-CS NPs (F1), RX-CS NPs (F2), and RX-HA-CS NPs treatments (Table 3). The IC_{50} values of RX-CS NPs (F1), RX-CS NPs (F2), and RX-HA-CS NPs for Caco-2 cells were 56.31 μM, 61.06 μM, and 25.45 μM, with 1.14, 1.05, and 2.52 cytotoxic fold changes, as well as 0.88, 0.95, and 0.40 IC_{50} fold changes, respectively. The IC_{50} values of RX-CS NPs (F1), RX-CS NPs (F2), and RX-HA-CS NPs for HCT116 cells were 45.59 μM, 54.10 μM, and 40.22 μM, with 1.90, 1.60, and 2.16 cytotoxic fold changes, as well as 0.53, 0.62, and 0.46 IC_{50} fold changes, respectively (Table 3).

For 48 h incubation, the IC50 values of RX-CS NPs (F1), RX-CS NPs (F2), and RX-HA-CS NPs for Caco-2 cells were 46.23 μM, 49.99 μM, and 20.61, respectively. The IC50 values of RX-CS NPs (F1), RX-CS NPs (F2), and RX-HA-CS NPs for HCT116 cells were 35.27 μM, 44.03 μM, and 36.65, respectively (Table 4). The fold change of the RX-HA-CS NPs reached 2.717 for Caco-2 cells and 2.166 for HCT 116 cells. Intriguingly, the RX-HA-CS NPs recorded undetectable IC_{50} and not detected (ND) result on WI-38 cells after 48 h incubation similar to the 24 h incubation period.

LncRNAs and miRNAs

The lncRNAs and miRNAs fold changes of Caco-2 were shown in Fig. 6A, B. Their fold changes in HCT 116 were shown in Fig. 6C, D cells versus normal cells. Some of the epigenetic panel of the LncRNAs, including H-19, HOTTIP, HULC, and LINC00641, were illustrated in Caco-2 and HCT116 cells upon RX and RX-HA-CS NPs (RX NP) treatments compared to undiseased cells. The expressions of HOTTIP,
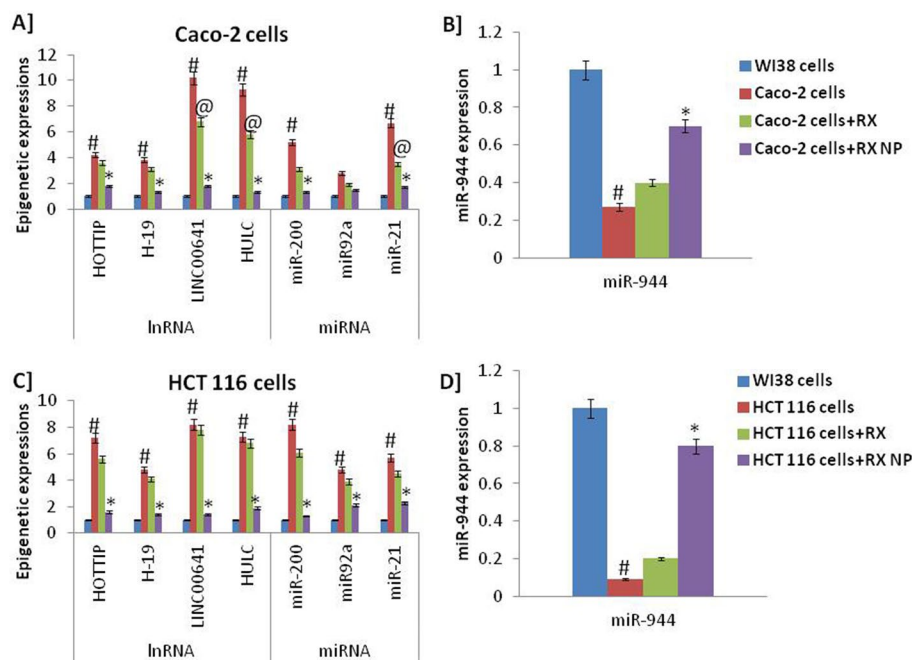
Fig. 6 The noncoding RNAs (lnRNAs and miRNAs) of Caco-2 (**A**, **B**) and HCT 116 (**C**, **D**) colorectal cancer cells versus WI-38 normal cells. The symbols #, @, and * represent significant differences as declared in "*Statistical analysis*" section

HULC, H-19, and LINC00641 were highly overexpressed ($p < 0.01$) in CRC cells from 3.8 times for H-19 to 10.2 times for LINC00641 in Caco-2 cells, as well as from 4.8 times for H-19 to 8.2 times for LINC00641 in HCT116 cells. miR-200, miR-21, and miR-92a (Fig. 6) were estimated in Caco-2 and HCT116 cells upon RX and RX NP therapies. The miRNAs expressions of Caco-2 and HCT116 cancer cells were examined after normalized to the normal cells. The miR-21, miR-200, and miR-92a were significantly ($p < 0.01$) overexpressed in CRC cell lines. In Caco-2, miR-92a expression was 2.8 and that of miR-21, it was 6.7. Meanwhile, fold change in HCT116 cells was 4.8 and 8.2 for miR-92a and miR-200, respectively.

LncRNA and miRNA overexpressions in both cancer cells were down-regulated using RX regimens, especially when RX NP was administered. The normal cells also were used in normalization. The lowest HOTTIP, H-19, LINC00641, HULC, miR-200, miR-21, and miR-92a expressions were reached when the RX NP was applied, reaching 1.8, 1.3, 1.8, 1.3,1.3–1.5, and 1.7 fold changes in Caco-2 cells and 1.6, 1.4, 1.4, 1.9, 1.3, 2.1, and 2.3 fold changes in HCT116 cells, respectively (Fig. 6).

Table 5 shows the comparison of the expression of lncRNA in treated Caco-2 and HCT116 cancer cells with that in untreated cells. Following RX treatments, cancer cells' expression levels of the lncRNAs H-19, HOTTIP, HULC, and LINC00641 were down-regulated. When lncRNAs expression was normalized to untreated cancerous cells, RX NP treatment resulted in the lowest expression levels, which were 0.43, 0.34, 0.18, and 0.14 fold changes in Caco-2 cell line and 0.22, 0.29, 0.17, and 0.26 fold changes in HCT116 cell line, respectively.

Table 5 The normalized long noncoding lnRNA, micro-RNA, and protein expressions of treated Caco-2 and HCT 116 colorectal cancerous cells versus the untreated ones

Parameters	RNAs/ proteins	Caco-2 cell line			HCT 116 cell line		
		Caco-2 cells	Caco-2 cells + RX	Caco-2 cells + RX NP	HCT 116 cells	HCT 116 cells + RX	HCT 116 cells + RX NP
lnRNAs	HOTTIP	1	0.86	0.43	1	0.78	0.22
	H-19	1	0.82	0.34	1	0.85	0.29
	LINC00641	1	0.67	0.18	1	0.95	0.17
	HULC	1	0.62	0.14	1	0.93	0.26
miRNAs	miR-200	1	0.60	0.25	1	0.74	0.16
	miR92a	1	0.68	0.54	1	0.81	0.44
	miR-21	1	0.52	0.25	1	0.79	0.40
	miR-944	1	2.00	3.50	1	2.22	8.89
Proteins	PPAR-γ	1	1.12	0.75	1	1.22	0.51
	VEGF	1	1.05	0.60	1	0.83	0.43
	YKL-40	1	1.04	0.76	1	0.90	0.63
	E-cadherin	1	0.92	1.75	1	0.82	2.18

Table 5 shows the comparison of the expression of miRNAs in treated Caco-2 and HCT116 cancer cells with that in the untreated cells. After applying RX regimens, Caco-2 and HCT116 cells had lower expression levels of miR-21,-200, and -92a. RX NP treatment resulted in the lowest levels of miR-200, -21, and -92a expression, with fold changes of 0.25, 0.54, and 0.25 in Caco-2 cell line and 0.16, 0.44, and 0.40 in HCT116 cell line, respectively.

Figure 6 displays the expression of miR-944 in each proposed cell line. In both untreated and treated human CRC cells, the expression of miR-944 was assessed and compared to that of healthy WI-38 cells. When compared to normal cells, the expression of miR-944 was significantly ($p < 0.01$) down-regulated in CRC cells. Then, this down-regulation was up-regulated significantly ($p < 0.01$) in Caco-2 and HCT116 cancerous cells after treatment with RX regimens especially when RX NP was tested. RX NP treatment resulted in the highest levels of miR-944 expression, which reached 3.50 fold change in Caco-2 cell line and 8.89 fold change in HCT116 cell line.

Protein levels

PPAR-γ, ECN, VEGF, and YKL-40 (Fig. 7A–D) protein expressions in Caco-2 (Fig. 4A, B) and HCT116 (Fig. 7C, D) colorectal cancer cells against WI-38 cell line were measured upon RX and RX NP treatments.

The expressions of the proposed PPAR-γ, VEGF, and YKL-40 were highly over-expressed significantly ($p < 0.01$) in CRC cells compared to normal cells. Using RX regimens, high expression levels of these proteins in both colon cancer cells were dramatically reduced, especially when RX NP was introduced. The lowest PPAR-γ, VEGF, and YKL-40 expressions were reached when RX NP was applied, reaching 50, 171, and 113 ng/mL versus untreated Caco-2 cell lines (67, 287, and 148 ng/mL), and 40, 150, and 105 ng/mL versus untreated HCT116 cell lines (78, 346, and 167.5 ng/mL), respectively (Fig. 7).
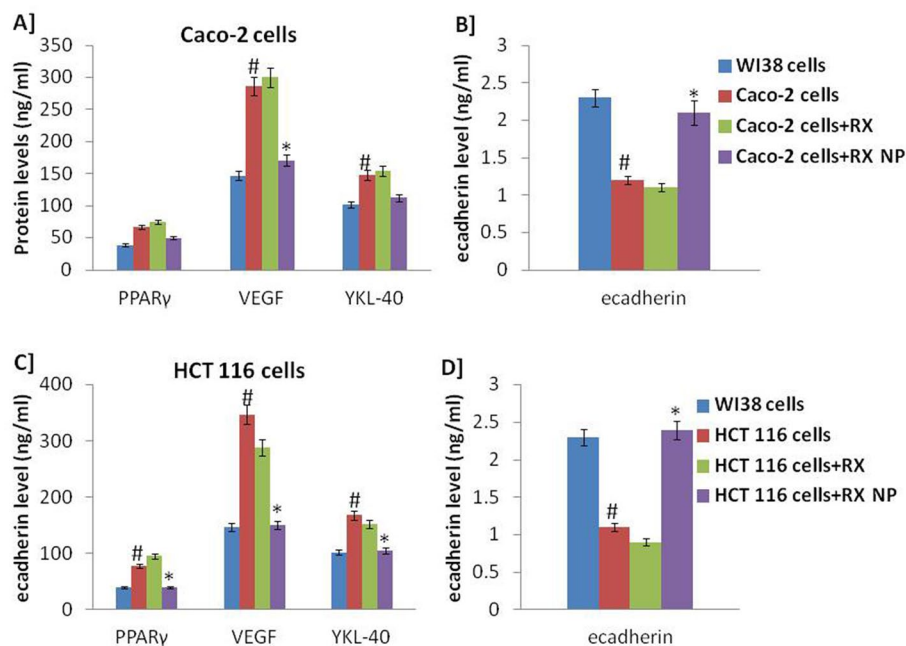
Fig. 7 The PPAR-γ, VEGF, YKL-40 (**A**, **C**), and E-cadherin (**B**, **D**) protein expressions of Caco-2 (A, B) and HCT116 (C, D) colorectal cancerous cells versus WI-38 normal cells. The symbols #, @, and * represent significant differences as declared in "*Statistical analysis*" section

Figure 4B, D shows the ECN expression of WI-38 healthy cells versus colon cancer cells. In CRC cells, ECN expression was down-regulated considerably ($p < 0.01$). In colon cancer cells, the low ECN expression levels were increased by RX regimens, particularly when RX NP was used. RX NP treatment resulted in the highest ECN expression, which was 2.2 ng/mL in Caco-2 cell line and 2.4 ng/mL in HCT116 cell line.

Eventually, the ECN concentration in cancerous cell lines was up-regulated upon RX regimens application, especially when RX NP was tested. The highest ECN expression was achieved when RX NP was applied, reaching 1.75 fold change in Caco-2 cell line and 1.75 fold change in HCT116 cell line (Table 5).

Discussion

Our observations were very promising in the field of targeted therapy of colorectal cancer. We used specific HA NPs which were specifically targeting the CD44-expressed cancer cells. Intriguingly, this targeted NPs induced higher cytotoxic effect and binding affinity to CD44 receptors against Caco-2 cell line than HCT 116 cell line. Post-treatment, the epigenetic mechanistic pathway was tracked and showed down-regulation of the expressions of H-19, HULC, HOTTIP, LINC00641, miR-92a, miR-200, miR-21, PPARγ, YKL-40, and VEGF, as well as up-regulation of the expressions of ECN and miR-944.

HA is a ligand for CD44 receptors found on the surface of the cancerous cells. Cancer therapy has been shown to be effective when selectively targeting theses over-expressed receptors (Mattheolabakis et al. 2012; Resnick et al. 1998; Shipitsin et al. 2007). CD44 receptors have a major impact on tumour growth (Hiscox et al. 2012),

metastasis (Hiraga et al. 2013), and treatment resistance (Gvozdenovic et al. 2013), making them one of the most attractive cancer therapeutic targets (Resnick et al. 1998; Shipitsin et al. 2007).

RX was constructed as a unique delivery system as an anticancer agent and CS as a polymeric nanoparticle. HA was used as an alternate route for direct drug administration. The hydrophobic or positively charged moieties were conjugated onto the hydrophilic backbone of the NPs in order to give them the self-assembling capabilities of RX-HA-CS NPs.

Younga´Choi and his colleagues (Younga'Choi et al. 2009) employed 5b-cholanic acid as a hydrophobic component that was conjugated to the backbone of HA to aid in nanoparticle self-assembly. The particle size of the produced nanoparticles was estimated to be between 350 and 400 nm, according to their findings. When HA NPs were labelled with the Cy5.5 stain, imaging revealed that they penetrated cancer cells more effectively than free HA polymer. Another study compared the ability of self-assembled HA nanoparticles to penetrate tumours, and it revealed that smaller particles were more effectively than their larger counterparts (Choi et al. 2010).

Recently, we observed that the average nano-sizes of CS NPs, HA-CS NPs, RX-CS NPs, and RX-HA-CS NPs were 176.6 ± 6.4 nm, 198.2 ± 7.7 nm, 210.6 ± 4.4 nm, and 208.7 ± 4.7 nm, respectively. Some modifications of the preparation method of CS NPs, HA-CS NPs, RX-CS NPs, and RX-HA-CS NPs regarding nano-ingredient change allowed us, in the current article, to decrease the average nano-sizes of the NPs (F1), 98.5 ± 7.3 nm, 118.2 ± 7.7 nm, 102.5 ± 5.5 nm, 114.5 ± 5.6 nm, which were in line with the existing NPs' physicochemical features.

Over the course of 28 h, the cumulative percentages of RX released from RX-CS NP (F1), RX-CS NP (F2), and RX-HA-CS NP were observed. With the best sustained release profiling, 20% of the entrapped RX was released after 6 h prior to the trial, and it remained generally constant at 20% over the 28 h. From 1 to 6 h, both formulae of RX-CS NPs showed the same release patterns, reaching roughly 30% of the entrapped RX. After 6 h, the RX release increased until it reached its maximum (65% for F2 and 50% for F1) at 24 h.

As the CS is positively charged, means cationic, and the used anionic negative chains of the PVA are very low in F1, the CS NP (F1) manufacturing process results in positively charged on the surface of the nanoparticles. Meanwhile, using higher amount of anionic chains of PVA in F2, the CS NP (F2) manufacturing process results in negatively charged ZPs on the NP surface. The negative acetate groups in the integrated PVA are thought to be the reason of the negative signs in CS NPs (F2). These acetate groups were previously thought to be important for PVA adsorption levels (Wiśniewska et al. 2016). The presence of positive charge on the membranes of HA-CS NPs and RX-HA-CS NPs similar to LC-CS NPs (Almutairi et al. 2019) could be attributed to a higher percentage of the positive CS used in comparison to the PVA.

Raloxifene (RX), an ER-selective medication, has not yet been properly investigated in colorectal cancer. Both colorectal cancer cells, HCT 116 and Caco-2, were evaluated for ER expression, and it was observed that Caco-2 cells have higher ER expression than HCT 116 cells. Scientists revealed that ER promotes colon cancer and that RX serves as an ER antagonist, offering colorectal cancer protection (Tolba et al. 2015).

The present corpus of work has mostly focused on HA-based CD44 receptor targeting in colorectal HCT 116 and Caco-2 cells as well as the release of RX as a potential anti-cancer drug from the RX-HA-CS NPs' shell. In the current study, Caco-2 cells were sensitive but HCT 116 cells were resistant to the RX regimens, especially the RX-HA-CS NPs, may be due to the ER selectivity as mentioned above (Tolba et al. 2015).

Anti-CD44 therapy utilizing ligands (e.g. HA) has progressed significantly in cancer therapies, resulting in the induction of an apoptotic cascade (Mattheolabakis et al. 2015). An anti-CD44 monoclonal antibody (mAb) was previously reported to be capable of releasing the halted differentiation of acute myeloid leukaemia cells and inducing death (Song et al. 2004). Furthermore, there was a considerable decrease in c-Myc expression, which was the anti-CD44 antibody's assigned mechanism of action (Song et al. 2004).

Anti-CD44 mAb (H90 and A3D8) displayed equivalent action in all five subtypes of AML in a similar study, demonstrating the efficacy and adaptability of this strategy. Several previous RX treatment regimen investigations revealed that this platform is cytotoxic against breast cancer (Gadhoum et al. 2004; Jordan et al. 1987; Ettinger et al. 1999) and lower reproductive tract malignancies (Kleinberg et al. 1983; Jordan 2001). The current study, on the other hand, is the first to look at the effect of RX in its HA-CS nano-formulation on CRC cancer cells. RX's major approved indication prior to 2007 was for osteoporosis prevention and therapy. In a trial looked into RX's anti-cancer properties, it was found that RX is equally effective as Tamoxifen in the therapy of metastatic cancer, with a lower risk of strock (Jordan 2001; Ettinger et al. 1999).

There is a significant need for new biomarkers with diagnostic potential. The fascinating importance of lncRNAs and miRNAs in CRC as prognostic as well as diagnostic displays, as well as their potential targets, has been highlighted. Similar to our study, there is a link between AMPK and PPAR-γ in providing anti-proliferative properties in malignant cells (Elmaci et al. 2016). In a previous study (Suhaimi et al. 2017), RX regimens inhibited VEGF, providing it as an anti-angiogenic agent. Previous studies were came in parallel with the current study, in which RX significantly decreased VEGF, PPAR-γ, and YKL-40 concentrations in cancer cells and RX nano-regimens significantly reduced PPAR-γ, VEGF, and YKL-40 expression levels in HCT116 and Caco-2 cells, especially when RX-HA-CS NPs were utilized. This could be because the targetability of the HA chains to the cancerous cells' receptors, making it easier for the RX-HA-CS NPs to bind to cell membranes and permitting cancer to be targeted actively (Dang et al. 2020).

EMT has been related to carcinogenesis and gives cancer cells the ability to spread throughout the body by enhancing their mobility, invasion potential, and resistance to apoptosis triggers. These observations are consistent with current results (IdoLaskov et al. 2016), which showed that RX regimens increased ECN level and reduced EMT. When RX NP was given, the highest ECN expression was achieved. The RX nano-regimen decreases ECN level and other related factors, such as p-Smad3, p-mTOR, survivin, and TGF-β (Muhamad et al. 2019).

RX regimens, like MT formulations, inhibit the development of CRC cells by altering miRNAs that affect numerous signalling pathways. The treatment regimen inactivated Akt by increasing miR-145 (tumour suppressor) expression (Muhamad et al. 2019). MiR-944 was found to decrease tumour cell invasiveness in CRC (Liu et al. 2016), which is compatible with the findings on miR-944, which was increased by RX and further

boosted employing RX nano-regimens, particularly the RX NP. Oncogenes miR-92a, -200, and -21, on the other hand, were reduced, which were consistent with earlier findings (Muhamad et al. 2019).

There is a relationship between miRNAs and CRC progression because miRNAs can influence numerous signals in colon cancer, including Wnt. Catenin/Wnt signalling is regulated by miR-92, cell growth is regulated by miR-21 and miR-200c, cancer apoptosis is regulated by miR-195, cell cycle is regulated by miR-192, cell differentiation is regulated by miR-200c, and cell division is regulated by miR-200a/b/c (Mohammadi et al. 2016).

Several dysregulated lncRNAs have been linked to the development of a variety of cancers. In CRC, the genes H-19, HOTTIP, HULC, and LINC00641 are crucial. EMT is critical for cancer metastasis, and H-19 increases it. These findings support previous research demonstrating H-19 expression is elevated in CRC and other malignancies (Raveh et al. 2015).

LINC00641 is a functional lncRNA that regulates cell autophagy and has been associated to cancer prognosis. By regulating miR-197-3p14, LINC00641 reduces the progression of bladder cancer. According to a study released in 2021 (Xue et al. 2021), LINC00641 enhances CRC proliferation via miRNAs. Intriguingly, removing LINC00641 from CRC cells diminishes vitality, indicating LINC00641 stimulates cells (Xue et al. 2021). Sun et al. discovered that HOTTIP is increased in a breast cancer cell line and is connected to cell growth and death through HOXA11 modulation. The decrease in cell viability in the liver and lung caused by knocking down HOTTIP coincided with our current findings (Abd-Rabou et al. 2021a; Sun et al. 2018).

The lncRNA HULC was shown to be overexpressed in CRC (Xu et al. 2014). Previous study has demonstrated that lncRNAs may be employed as epigenetic indicators, notably in CRC patients treated with anti-VEGF targeted therapies (Abd-Rabou et al. 2021b; Garajov et al. 2017). H-19 and HULC were identified to target interleukin-6 and CXCR4, respectively, in cholangiocarcinoma cells, and were controlled by miRNAs. H-19 and HULC were found to be important modulators of other cancer-causing downstream inflammatory genes (Wen-Tao et al. 2016).

Conclusion

In conclusion, RX can be delivered to CRC cells using a HA-CS nano-platform in a targeted manner using HA-CD44 ligand-receptor connection strategy. RX nano-regimen (RX NP) may drastically suppress CRC cell formation in vitro, using HCT116 and Caco-2 cell lines, and this impact was higher than the free counterpart. The mechanistic pathway behind the anticancer activity of RX NP was mediated via epigenetics.

Study limitations and future prospective

We studied the CD44 receptor and the specific binding affinity with the labelled NPs which in turn allow the NPs to be internalized the cancer cells which got the highest binding affinity with CD44 receptors on colorectal cancer Caco-2 cell line. Intriguingly, the cellular uptake in Caco-2 cells was higher than HCT116 cells, compared with minimal uptake happened in case of normal WI-38 cells. These observations confirmed the cytotoxicity data against Caco-2, HCT116, and WI-38 cell lines. Future in vivo studies

should be considered to approve the concept of the targeted therapy and overcome the in vitro limitations.

Availability of data and materials
The data sets used and/or analysed during this study are available from the corresponding author on reasonable request.

Declarations

Ethics approval and consent to participate
All experiments were performed based on in vitro assays.

Consent for publication
Not applicable.

Competing interests
The authors declare that the authors have no competing interests.

Published online: 07 April 2023

References
Abdelaleem OO, Shaker OG, AbdelHafez MN, Abdelghaffar NK, Eid HM, Zaidan M, Khalefa AA, Ahmed NA, Hemeda NF, Zaki OM, Awaji AA, Mohammed SR (2012) The influence of rs1859168 polymorphism on serum expression of HOT-TIP and Its target miR-615-3p in Egyptian patients with breast cancer. Biomolecules 11:733

Abd-Rabou AA, Ahmed HH (2017) CS-PEG decorated PLGA nano-prototype for delivery of bioactive compounds: A novel approach for induction of apoptosis in HepG2 cell line. Adv Med Sci 2017(62):357–367

Abd-Rabou AA, Edris AE (2021) Cytotoxic, apoptotic, and genetic evaluations of *Nigella sativa* essential oil nanoemulsion against human hepatocellular carcinoma cell lines. Cancer Nanotechnol 12(1):1–23

Abd-Rabou AA, Edris AE (2022) Frankincense essential oil nanoemulsion specifically induces lung cancer apoptosis and inhibits survival pathways. Cancer Nanotechnol 13(1):1–24

Abd-Rabou AA, Mwaheb MA, Sayed ON et al (2017) 5-fluorouracil synergized with raloxifene and cytosine β-ᴅ-arabinofuranoside to combat colorectal cancers in vitro via controlling lipolysis. J Pharmacol Toxicol 12(1):14–23

Abd-Rabou AA, Abd El-Salam NM, Sharada HMI et al (2021a) Thymoquinone crosstalks with DR5 to sensitize TRAIL resistance and stimulate ROS-mediated cancer apoptosis. Asian Pac J Cancer Prev APJCP 22(9):2855

Abd-Rabou AA, Abdelaziz AM, Shaker OG, Ayeldeen G (2021b) Metformin-loaded lecithin nanoparticles induce colorectal cancer cytotoxicity via epigenetic modulation of noncoding RNAs. Mol Biol Rep 48(10):6805–6820

Abd-Rabou AA, Ahmed HH, Kishta MS (2022a) Implication of extrinsic and intrinsic apoptotic pathways in the targeted therapy of hepatocellular carcinoma using aptamer-labeled viramidine nanoparticles. BMC Cancer 22(1):1–14

Abd-Rabou AA, Ahmed HH, Kishta MS, Zoheir K (2022b) Selective viramidine-loaded aptamer-nanoparticles trigger cell cycle arrest in nucleolin-expressed hepatoma cells through modulation of CDC25A/p53/PI3k pathway. J Clust Sci 34:1–14

Almutairi FM, Abd-Rabou AA, Mohamed MS (2019) Raloxifene-encapsulated hyaluronic acid-decorated chitosan nanoparticles selectively induce apoptosis in lung cancer cells. Bioorg Med Chem 27:1629–1638

Bikiaris D, Karavelidis V, Karavas E (2009) Novel biodegradable polyesters synthesis and application as drug carriers for the preparation of raloxifene HCl loaded nanoparticles. Molecules 14(7):2410–2430

Carter JV, O'Brien SJ, Burton JF et al (2019) The microRNA-200 family acts as an oncogene in colorectal cancer by inhibiting the tumor suppressor RASSF2. Oncol Lett 18(4):3994–4007

Chinnaiyan SK, Karthikeyan D, Gadela VR (2018) Development and characterization of metformin loaded pectin nanoparticles for T2 diabetes mellitus. Pharm Nanotechnol 6:253–263

Choi KY, Chung H, Min KH et al (2010) Self-assembled hyaluronic acid nanoparticles for active tumor targeting. Biomaterials 31:106–114

Dang Y, Guan J (2020) Nanoparticle-based drug delivery systems for cancer therapy. Smart Mat in Med 1:10–19

El-Hamed A, Abd-Rabou AA, Faramawy A (2022) Therapeutic efficacy of curcuma and pomelo loaded chitosan nanoparticles in intestinal murine trichinellosis. Egypt J Chem 65(2):551–564

Elmaci İ, Altinoz MA (2016) A Metabolic inhibitory cocktail for grave cancers: metformin, pioglitazone and lithium combination in treatment of pancreatic cancer and glioblastoma multiforme. Biochem Genet 54(5):573–618

Ettinger B, Black DM, Mitlak BH et al (1999) Reduction of vertebral fracture risk in postmenopausal women with osteoporosis treated with raloxifene: results from a 3-year randomized clinical trial. JAMA 282:637–645

Fontana MC, Beckenkamp A, Buffon A et al (2014) Controlled release of raloxifene by nanoencapsulation: effect on in vitro antiproliferative activity of human breast cancer cells. Int J Nanomedicine 9(1):2979–2991

Gadhoum Z, Delaunay J, Maquarre E et al (2004) The effect of anti- CD44 monoclonal antibodies on differentiation and proliferation of human acute myeloid leukemia cells. Leuk Lymphoma 45:1501–1510

Garajov I, Ferracin M, Porcellini E, Palloni A, Abbati F, Biasco G, Brandi G (2017) Non-coding RNAs as predictive biomarkers to current treatment in metastatic colorectal cancer. In J Mol Sci 18:1547

Gvozdenovic A, Arlt MJ, Campanile C et al (2013) CD44 enhances tumor formation and lung metastasis in experimental osteosarcoma and is an additional predictor for poor patient outcome. J Bone Miner Res 28:838–847

Hashim AF, Abd-Rabou AA, El-Sayed HS (2022) Functional nanoemulsion and nanocomposite microparticles as an anticolorectal cancer and antimicrobial agent: applied in yogurt. Biomass Conv Bioref. https://doi.org/10.1007/s13399-022-03313-3

Hiraga T, Ito S, Nakamura H (2013) Cancer stem-like cell marker CD44 promotes bone metastases by enhancing tumorigenicity, cell motility, and hyaluronan production. Cancer Res 73:4112–4122

Hiscox S, Baruha B, Smith C et al (2012) Overexpression of CD44 accompanies acquired tamoxifen resistance in MCF7 cells and augments their sensitivity to the stromal factors, heregulin and hyaluronan. BMC Cancer 12:458

IdoLaskov I, Paul A, Oreekha A, Charles-Andre P, Marie-Claude B, Amber Y, Walter H (2016) Metformin increases E-cadherin in tumors of diabetic patients with endometrial cancer and suppresses epithelial-mesenchymal transition in endometrial cancer cell lines. Int J Gynecol Cancer 26(7):1213–1221

Jordan VC (2001) Selective estrogen receptor modulation: a personal perspective. Cancer Res 61:5683–5687

Jordan VC, Phelps E, Lindgren JU (1987) Effects of anti-estrogens on bone in castrated and intact female rats. Breast Cancer Res Treat 10:31–35

Kleinberg DL, Todd J, Babitsky G (1983) Inhibition by estradiol of the lactogenic effect of prolactin in primate mammary tissue: reversal by antiestrogens LY 156758 and tamoxifen. Proc Natl Acad Sci USA 80:4144–4148

Liu M, Zhou K, Cao Y (2016) MicroRNA-944 affects cell growth by targeting EPHA7 in non-small cell lung cancer. Int J Mol Sci 17(10):1493

Lizarbe MA, Calle-Espinosa J, Fernández-Lizarbe E, Fernández-Lizarbe S, Robles MÁ, Olmo N, Turnay J (2017) Colorectal cancer: from the genetic model to posttranscriptional regulation by noncoding RNAs. Biomed Res Int 2017:7354260

Mattheolabakis G, Rigas B, Constantinides PP (2012) Nanodelivery strategies in cancer chemotherapy: biological rationale and pharmaceutical perspectives. Nanomedicine 7:1577–1590

Mattheolabakis G, Milane L, Singh A et al (2015) Hyaluronic acid targeting of CD44 for cancer therapy: from receptor biology to nanomedicine. J Drug Target 23(7–8):605–618

Meng F, Song L, Wang W (2017) Metformin improves overall survival of colorectal cancer patients with diabetes: a meta-analysis. J Diabetes Res 2017:5063239

Mohammadi A, Mansoori B, Baradaran B (2016) The role of microRNAs in colorectal cancer. Biomed Pharmacother 84:705–713

Muhamad N, Moklesur RS, Jin-Rong Z (2019) Metformin in colorectal cancer: molecularmechanism, preclinical and clinical aspects. J Exp Clin Cancer Res 38:491

Parveen S, Sahoo SK (2011) Long circulating chitosan/PEG blended PLGA nanoparticle for tumor drug delivery. Eur J Pharmacol 670:372–383

Raveh E, Matouk IJ, Gilon M, Hochberg A (2015) The H19 Long non-coding RNA in cancer initiation, progression and metastasis—a proposed unifying theory. Mol Cancer 14:184

Resnick NM, Clarke MR, Siegfried JM et al (1998) Expression of the cell adhesion molecule CD44 in human lung tumors and cell lines. Mol Diagn 3:93–103

Schee K, Boye K, Abrahamsen TW et al (2012) Clinical relevance of microRNA miR-21, miR-31, miR-92a, miR-101, miR-106a and miR-145 in colorectal cancer. BMC Cancer 12:505

Shaker OG, Senousy MA, Elbaz EM (2017) Association of rs6983267 at 8q24, HULC rs7763881 polymorphisms and serum lncRNAs CCAT2 and HULC with colorectal cancer in Egyptian patients. Sci Rep 7:16246

Shipitsin M, Campbell LL, Argani P et al (2007) Molecular definition of breast tumor heterogeneity. Cancer Cell 11:259–273

Siddiqui H, Al-Ghafari A, Choudhry H, Al Doghaither H (2019) Roles of long non-coding RNAs in colorectal cancer tumorigenesis: a review. Mol Clin Oncol 11(2):167–172

Song G, Liao X, Zhou L et al (2004) HI44a, an anti-CD44 monoclonal antibody, induces differentiation and apoptosis of human acute myeloid leukemia cells. Leukemia Res 28:1089–1096

Sporn MB, Dowsett SA, Mershon J et al (2004) Role of raloxifene in breast cancer prevention in postmenopausal women: clinical evidence and potential mechanisms of action. Clin Ther 26(6):830–840

Suchaoin W, Bernkop-Schnürch AS (2017) Nanocarriers protecting toward an intestinal pre-uptake metabolism. Nanomedicine 12(3):255–269

Suhaimi NA, Phyo WM, Yap HY, Choy SH, Wei X, Choudhury Y et al (2017) Metformin inhibits cellular proliferation and bioenergetics in colorectal cancer patient–derived Xenografts. Mol Cancer Ther 16(9):2035–2044

Sun Y, Zeng C, Gan S, Li H, Cheng Y, Chen D (2018) LncRNA HOTTIP-mediated HOXA11 expression promotes cell growth, migration and inhibits cell apoptosis in breast cancer. Int J Mol Sci 19:472

Tolba MF, Abdel-Rahman SZ (2015) Pterostilbine, an active component of blueberries, sensitizes colon cancer cells to 5-fluorouracil cytotoxicity. Sci Rep 5:15239

Van Meerloo J, Kaspers GJ, Cloos J (2011) Cell sensitivity assays: the MTT assay. Methods Mol Biol 731:237–245

Wang WT, Ye H, Wei PP, Han BW, He B, Chen ZH, Chen YQ (2016) LncRNAs H19 and HULC, activated by oxidative stress, promote cell migration and invasion in cholangiocarcinoma through a ceRNA manner. J Hematol Oncol 9(1):117

Wiśniewska M, Bogatyrov V, Ostolska I, Szewczuk-Karpisz K, Terpiłowski K, Nosal-Wiercińska A (2016) Impact of poly(vinyl alcohol) adsorption on the surface characteristics of mixed oxide Mn xOy–SiO2. Adsorption 22:417–423

Xu MD, Qi P, Du X (2014) Long non-coding RNAs in colorectal cancer: implications for pathogenesis and clinical application. Mod Pathol 27:1310–1320

Xue D, Xue YF, Zhang LJ, Cui LZ, Guo KQ, Lian J (2021) LINC00641 induces the malignant progression of colorectal carcinoma through the miRNA-424-5p/PLSCR4 feedback loop. Eur Rev Med Pharmacol Sci 25(2):749–757

Younga'Choi K, Hyuna'Min K, Heea'Na J et al (2009) Self-assembled hyaluronic acid nanoparticles as a potential drug carrier for cancer therapy: synthesis, characterization, and in vivo biodistribution. J Mater Chem 19:4102–4117

Zhang RX, Ahmed T, Li LY et al (2017) Design of nanocarriers for nanoscale drug delivery to enhance cancer treatment using hybrid polymer and lipid building blocks. Nanoscale 9(4):1334–1355

Publisher's Note